

# Quantification of regional myocardial wall motion by cardiovascular magnetic resonance

Kai Jiang<sup>1,2</sup>, Xin Yu<sup>1,2,3,4</sup>

<sup>1</sup>Departments of Biomedical Engineering, <sup>2</sup>Case Center for Imaging Research, <sup>3</sup>Radiology, and <sup>4</sup>Physiology and Biophysics, Case Western Reserve University, Cleveland, Ohio, USA

*Correspondence to:* Xin Yu, Sc.D. Wickenden 430, 10900 Euclid Avenue, Cleveland, OH, 44106, USA. Email: xin.yu@case.edu.

**Abstract:** Cardiovascular magnetic resonance (CMR) is a versatile tool that also allows comprehensive and accurate measurement of both global and regional myocardial contraction. Quantification of regional wall motion parameters, such as strain, strain rate, twist and torsion, has been shown to be more sensitive to early-stage functional alterations. Since the invention of CMR tagging by magnetization saturation in 1988, several CMR techniques have been developed to enable the measurement of regional myocardial wall motion, including myocardial tissue tagging, phase contrast mapping, displacement encoding with stimulated echoes (DENSE), and strain encoded (SENC) imaging. These techniques have been developed with their own advantages and limitations. In this review, two widely used and closely related CMR techniques, i.e., tissue tagging and DENSE, will be discussed from the perspective of pulse sequence development and image-processing techniques. The clinical and preclinical applications of tissue tagging and DENSE in assessing wall motion mechanics in both normal and diseased hearts, including coronary artery diseases, hypertrophic cardiomyopathy, aortic stenosis, and Duchenne muscular dystrophies, will be discussed.

**Keywords:** Cardiovascular disease (CVD); cardiovascular magnetic resonance (CMR); MR tissue tagging; displacement-encoding with stimulated echoes (DENSE)

Submitted Sep 07, 2014. Accepted for publication Sep 12, 2014.

doi: 10.3978/j.issn.2223-4292.2014.09.01

**View this article at:** <http://dx.doi.org/10.3978/j.issn.2223-4292.2014.09.01>

## Introduction

Cardiovascular disease (CVD) is one of the leading causes of morbidity and mortality worldwide, accounting for approximately one third of all deaths in 2008 (1). A robust and accurate technique for early diagnosis of CVD is of significant clinical value by allowing preventive interventions. Although global myocardial parameters such as left-ventricular (LV) ejection fraction and stroke volume serve as a good indicator of CVD, the analysis of regional myocardial wall motion has emerged as more sensitive measures of early-stage functional alterations.

Computer-aided fluoroscopy in combination with the implantation of radiopaque markers has been used for the measurement of LV wall motion (2). However, such method is highly invasive and is not practical for large scale clinical use. Electrocardiography (ECG)-gated SPECT was also developed

to measure global and regional wall motion but nevertheless suffers from limited spatial and temporal resolution (3). The echocardiographic techniques, such as tissue Doppler imaging (TDI) (4) and speckle tracking (5), were developed for noninvasive quantification of myocardial strain at high temporal resolution (>250 frames/s) and have been used in clinical studies. However, both methods are operator dependent and are limited by poor acoustic windows. Thus, an imaging modality, which can noninvasively and accurately measures myocardial wall motion, will greatly facilitate the diagnosis, prognosis, and management of cardiac diseases.

Cardiovascular magnetic resonance (CMR) provides a unique tool for non-invasive and accurate measurement of regional cardiac function. Since the invention of CMR tagging by magnetization saturation in 1988 (6), several CMR techniques have been developed to enable the measurement

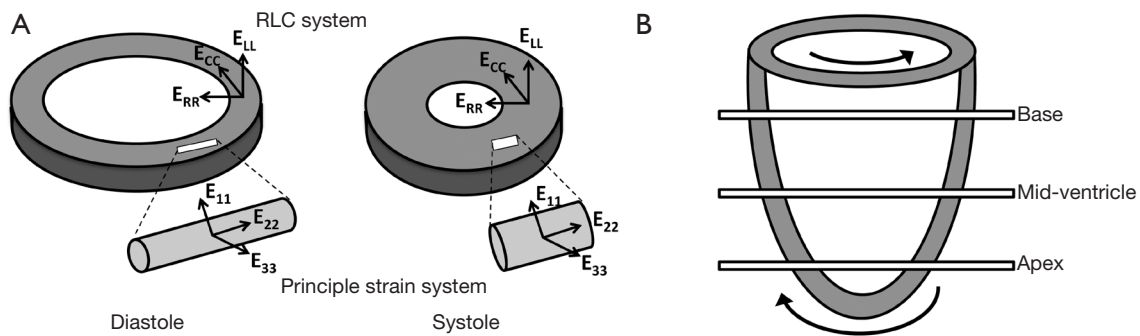


**Figure 1** Deformation of left ventricular (LV) myocardium during contraction. (A) Myocardial wall strains in Radial-Circumferential-Longitudinal (RCL) and the principal systems. The RCL system uses the geometry of the heart to define three orthogonal strains. The radial strain ( $E_{RR}$ ), circumferential strain ( $E_{CC}$ ), and longitudinal strain ( $E_{LL}$ ) describe the LV wall thickening in the radial direction and shortening in the circumferential and longitudinal directions, respectively. The principal strain system uses myocardial fiber geometry to define three orthogonal strains.  $E_{11}$  is along the direction of greatest length increase in myofiber and  $E_{22}$  is along the direction of greatest length decrease in myofiber.  $E_{33}$  is along the direction orthogonal to both  $E_{11}$  and  $E_{22}$ . (B) LV wall undergoes a torsional deformation during contraction with the apex twists counterclockwise and the base twists clockwise (viewing from apex to base).

of mechanical parameters that describe regional myocardial wall motion such as strain, strain rate, twist, and torsion. In this review, we will focus our discussion on two widely used and closely related CMR techniques, tissue tagging and displacement encoding with stimulated echoes (DENSE). The clinical and preclinical applications of these methods in both normal and diseased hearts, including coronary artery diseases, hypertrophic cardiomyopathy, aortic stenosis, and Duchenne muscular dystrophies, will also be discussed.

### Quantification of regional myocardial deformation

The myofibers of mammalian hearts are organized in a unique pattern. These fibers change gradually from a right-handed helix in the subendocardium to a circumferential arrangement in the mid wall, then to a left-handed helix in the subepicardium. This intricate 3D fiber structure gives rise to a complex pattern of deformation during contraction. The LV shortens in the longitudinal direction while the ventricular wall thickens in the radial direction. In addition, the whole LV twists due to the opposite fiber orientation at endo- and epicardial wall (7). As such, a comprehensive assessment of myocardial wall deformation requires the measurements of several parameters.

#### Strain

The deformation of a single myofiber can be described by 1D strain, which is a measure of the fractional change in fiber

length. Similarly, the deformation of myocardial wall can be described by a 3D strain tensor. Two coordinate systems have been used to describe the 3D myocardial strain: the Radial-Circumferential-Longitudinal (RCL) system and the principal strain system (also known as the Fiber-Cross-Fiber system). There are three normal strains in the RCL system: the radial strain ( $E_{RR}$ ), the circumferential strain ( $E_{CC}$ ), and the longitudinal strain ( $E_{LL}$ ). While  $E_{RR}$  and  $E_{CC}$  describe myocardial thickening and shortening in the short-axis plane,  $E_{LL}$  measures LV shortening in the longitudinal direction (Figure 1A). In addition, strain changes that occur in a plane between two of these three orthogonal directions are referred to as the shear strains:  $E_{RC}$ ,  $E_{RL}$ , and  $E_{CL}$ , respectively. For example,  $E_{RC}$  represents the shear in the Radial-Circumferential plane.

Similarly, in the principal strain system,  $E_{11}$ ,  $E_{22}$ , and  $E_{33}$  are the three principal strains (Figure 1A). The principal strain system has the advantage of representing the complex material deformation regardless of cardiac geometry and the selected coordinate system (8). In contrast, the RCL system appears more intuitive since it is defined by the geometry of the heart. For both systems, a positive strain represents lengthening or thickening of the myocardium, whereas a negative strain represents shortening of the myocardium.

#### Strain rate

Strain rate is the rate of strain changes over the course of time. It has been widely used in both echocardiographic

and CMR measurements of LV function. Using strain rate as an index of LV regional function, previous studies have reported a significant decrease in the diastolic strain rate in patients with asymptomatic LV hypertrophy (9).

### *Twist and torsion*

In addition to myocardial thickening and shortening, the heart also undergoes a wringing motion during contraction due to the obliquely oriented subendocardial and subepicardial helices (7). Viewing from the apex of the heart, the base rotates in clockwise direction and the apex rotates counterclockwise (*Figure 1B*). This rotation of myocardial tissue is known as twist. Torsion is quantified as the difference in twist between apical and basal slices normalized by the gap between these two slices. Myocardial twist and torsion are affected by myofiber orientation (10), myocyte contractility (11), and the loading conditions (12). They have been shown to be sensitive to subtle changes in systolic and diastolic dysfunction. Stuber *et al.* reported an increased apical twist and ventricular torsion in patients suffering from pressure overload due to aortic stenosis. In addition, they observed a prolonged diastolic apical untwisting, which may contribute to a tendency toward diastolic dysfunction, in these patients (13).

## **CMR techniques for measurement of myocardial wall mechanics**

### *Myocardial tissue tagging*

Myocardial tissue tagging was first developed by Zerhouni *et al.* in 1988 (6). Noninvasive tissue markers, known as tags, are placed in myocardium (usually immediately after the detection of the R wave) by modulation of the magnetization. These tags follow the myocardial motion during contraction and can be detected by MR imaging. Since then, extensive research efforts have been devoted to the development of different tagging techniques. Although tissue tagging provides the potential for comprehensive assessment of myocardial wall motion, quantitative analysis of tag deformation has been laborious and time-consuming. A few semi-automated analysis methods, either magnitude based or phase based, have been developed to facilitate the analysis of tagged images.

### **Sequence development**

Early myocardial tissue tagging used magnetization saturation

to create fiducial markers in myocardium. Slice-selective radiofrequency (RF) pulses were applied perpendicular to the imaging plane to saturate the longitudinal magnetization at the intersection of the selected slices and the imaging plane. The saturated portion of the myocardium appeared dark in the images acquired subsequently. By tracking the movement of these dark lines, referred to as taglines, myocardial wall strain can be calculated (6). The validity of this technique in measuring myocardial wall motion was demonstrated by comparing it to sonomicrometry (14). However, this technique has some inherent limitations. First, a number of RF pulses need to be implemented sequentially to create multiple taglines, which increases the energy deposition to patients. Second, the sequential implementation of RF pulses creates non-uniform tag intensity. Further, only a few taglines can be generated after the detection of R-wave, thus, the tagging resolution is limited. Due to these limitations, this technique is not used widely.

Axel *et al.* (15) developed a more efficient tagging technique known as spatial modulation of magnetization (SPAMM). This technique adds sinusoidal modulation to the magnetization by applying only two equal-strength non-selective RF pulses, separated by a magnetization encoding gradient ( $G_{ENC}$ ) (*Figure 2A*). Tagging frequency is determined by the strength and duration of the encoding gradient; a larger and longer gradient induces higher tagging frequency. Shown in *Figure 2B* are representative short-axis and long-axis tagged images at end-diastole and peak systole, superimposed with traced taglines.

Sharper tagline profiles can be achieved by using higher order SPAMM methods, which uses a binomial combination of RF pulses instead of two RF pulses in 1-1 SPAMM (17). A similar technique using delays alternating with nutation for tailored excitation (DANTE) was developed by Mosher *et al.* (18), which used a train of RF pulses to generate sharper taglines. Subsequently, McVeigh *et al.* realized tagging with variable density for improved sampling of myocardial motion (19). However, one limitation of these methods is the long tagging preparation time than the original 1-1 SPAMM.

Regardless of the different tagging method in all these CMR techniques, they share a common issue: the fading of taglines due to  $T_1$  relaxation (*Figure 2B*). After the tagging module, the tagged tissue will restore the equilibrium magnetization at an exponential rate, which is determined by the longitudinal relaxation time  $T_1$ . As tagging module is typically applied at the beginning of systole after the detection of R-wave, the fading of taglines thereafter will

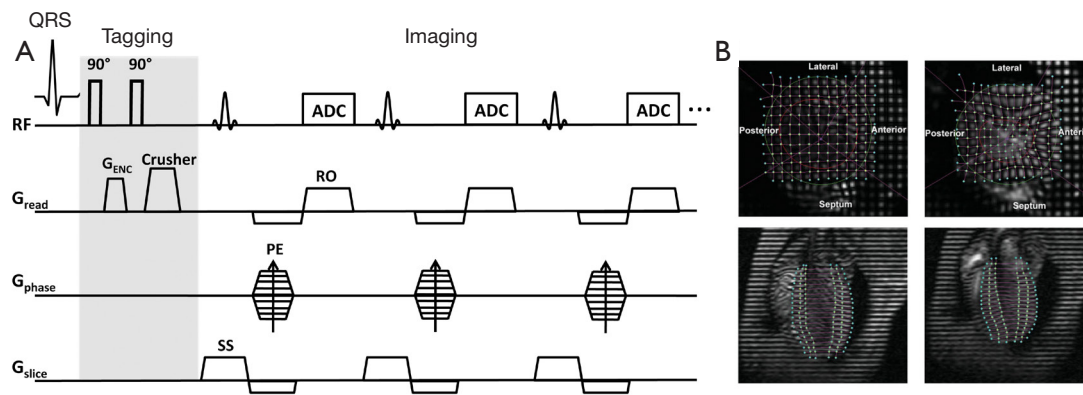


**Figure 2** MR tagging by SPAMM. (A) SPAMM pulse sequence; (B) representative short-axis (upper panels) and long-axis (lower panels) tagged images at end-diastole (left panels) and peak systole (right panels) superimposed with traced taglines [B is reproduced with permission from Zhong *et al.* (16)]. MR, magnetic resonance; SPAMM, spatial modulation of magnetization.

cause diminished tagging contrast during diastole, leading to inaccurate quantification of myocardial wall motion during late diastole. Implementation of the balanced steady state free precession (bSSFP) technique (20) and CMR tagging at high magnetic field strength (21), e.g., 3T, can offer better tagging contrast and longer tagging persistence. Nevertheless, the fading of taglines remains in general. Another issue associated with the conventional tagging method is the through-plane motion. When the heart contracts, myocardial motion occurs not only in the short-axis plane but also in the longitudinal direction. Therefore, a series of cine images acquired during a cardiac cycle comprises of images from different myocardial tissue (22). This through-plane motion can also give rise to inaccuracies in strain calculation. To resolve these issues, Fischer *et al.* developed complementary SPAMM (CSPAMM) (23). In addition to the original SPAMM scan, a second scan is acquired with the second 90° RF pulse inverted. By subtracting these two images, the recovered magnetization due to T<sub>1</sub> relaxation is removed. Further, the CSPAMM can also effectively solve the through-plane motion problem by using slice-selective RF pulses in the tagging module (24). However, these improvements are at the expense of doubled imaging acquisition time.

The deformation of the taglines is captured in the cine images acquired after the implementation of the tagging module. A high temporal resolution is desirable to delineate myocardial wall motion during the entire cardiac cycle, especially under stressed conditions. The gradient-echo (GRE) sequence is one of the most basic CMR imaging sequences. Segmented k-space GRE sequences

were developed to accelerate image acquisition without introducing significant artifacts (25,26). Echo planar imaging (EPI) (27-29) and bSSFP (20,30,31) sequences also showed their capability in improving imaging efficiency. Other encoding schemes, such as radial (32) and spiral (33) encoding, have also been performed in CMR tagging to improve spatial and temporal resolution. The development of parallel imaging techniques, such as simultaneous acquisition of spatial harmonics (SMASH) (34) and sensitivity encoding (SENSE) (35) provides further opportunity to accelerate image acquisition. The combination of CMR tagging with parallel imaging techniques brings great benefits to cardiac imaging by reducing the breath-hold duration and increasing the spatial resolution for a given breath-hold duration (36).

### Image analysis

The analysis of tagged CMR images can be divided into two stages, the tracking of taglines and the calculation of wall motion parameters. Several post-processing techniques have been developed for extracting and tracking myocardial tags. Algorithms such as Find Tags (37) or SPAMMVU (38) typically use manual or semi-automatic methods to identify the location of taglines and their intersecting points. Calculation of myocardial wall strain has used modeling approaches, including the finite element analysis (39,40), the volumetric modeling (41-43), the statistical modeling (40,44), and the 3D active contour modeling (45-48). Despite the apparent differences in these post-processing methods, they all require extensive user interaction and are very laborious and time consuming.

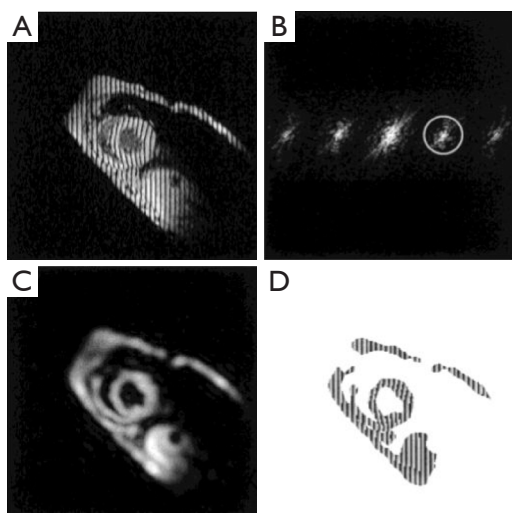


**Figure 3** HARP analysis of a tagged image. (A) An MR tagged image with vertical taglines; (B) the same tagged image in the k-space; (C,D) the magnitude (C) and phase image (D) after the inverse Fourier transform of the selected spectral peak in B. [Reproduced with permission from Osman *et al.* (49)]. HARP, harmonic phase; MR, magnetic resonance.

The harmonic phase (HARP) analysis is a phase-based method aimed at rapid and automated post-processing of tagged images (49). The sinusoidal modulation of the magnetization in the spatial domain by SPAMM sequence gives rise to spectral peaks at the multiples of the tagging frequency in the k-space (Figure 3). Tissue motion is directly encoded in the phase images of the off-center spectral peaks (harmonic peaks). Thus, taglines can be traced automatically by tracking the iso-phase contours in the phase images (50). Direct quantification of myocardial wall strain is also possible by calculating the gradient of the unwrapped phase images (51-54). Multiple validation studies have been conducted to demonstrate the robustness and accuracy of HARP analysis (14,52,55,56). HARP analysis can significantly decrease post-processing time and subjective user interference, which has made it the most attractive method for strain quantification in CMR tagging.

HARP analysis is highly sensitive to the size and shape of the filter used to extract the harmonic peaks, which inevitably affects the resolution of the reconstructed image and the accuracy of calculated strains. An elliptical filter with a Gaussian edge has been shown to be effective (51). In addition, simultaneous use of the positive and negative harmonic peaks has been shown to be effective in improving the SNR of HARP analysis (57). Finally, since the central peak of a CSPAMM image is eliminated, HARP analysis

of CSPAMM images offers more flexible filter choice and more accurate wall motion quantification (58).

The HARP method also provides the opportunity for real-time strain measurement. Since only the first-order harmonic peaks are required for strain quantification, only a small portion of the k-space needs to be sampled. As a result, scan time can be significantly reduced. Sampath *et al.* demonstrated real-time HARP by combining EPI with parallel imaging (59). A similar technique, known as FastHARP, was also developed for real-time measurement of strain at a rate of 25 frames/s (60).

### Displacement encoding with stimulated echoes (DENSE)

DENSE, a phase-based method for measuring tissue displacement, was developed in 1999 by Aletras *et al.* (61). Similar to HARP, tissue displacement is encoded directly in the phase of the stimulated echo in a DENSE image. A cine DENSE pulse sequence is shown in Figure 4A. The preparation module is a 1-1 SPAMM tagging sequence with an encoding gradient  $G_{ENC}$ . It is followed by an imaging module that includes a refocusing gradient ( $G_{DEC}$ ) that completely refocuses spin dephasing induced by the tagging gradient for stationary tissues. As such, moving spins will have an accumulative phase that is linearly proportional to the displacement that occurs between the tagging module and image readout. In the k-space, there are three distinct spectral peaks in a DENSE image, representing the stimulated echo, the  $T_1$  relaxation echo, and the stimulated anti-echo, respectively (Figure 4B). Tissue displacement is encoded in the phase of the stimulated echo. A representative displacement map of a mid-ventricular slice at peak systole is shown in Figure 4C. Similar to HARP, DENSE also has the advantages of fast image acquisition and data processing.

Strain quantification by DENSE is also impacted by the size of the filter used to extract the stimulated echo. Alternatively, the  $T_1$  relaxation echo and the stimulated anti-echo can be suppressed physically. The stimulated anti-echo can be removed by using a relatively large displacement-encoding gradient to shift it outside of the range of k-space sampling domain (Figure 5A,B). The inversion recovery technique has been used to suppress the  $T_1$  relaxation echo by nulling the signal for a particular  $T_1$  (Figure 5C,D). However, the stripe artifact is still present from tissue with other  $T_1$  values (Figure 5E,F) (64). In addition, this technique is not suitable for CINE DENSE. A more effective way of eliminating the  $T_1$  relaxation echo is to use the alternating

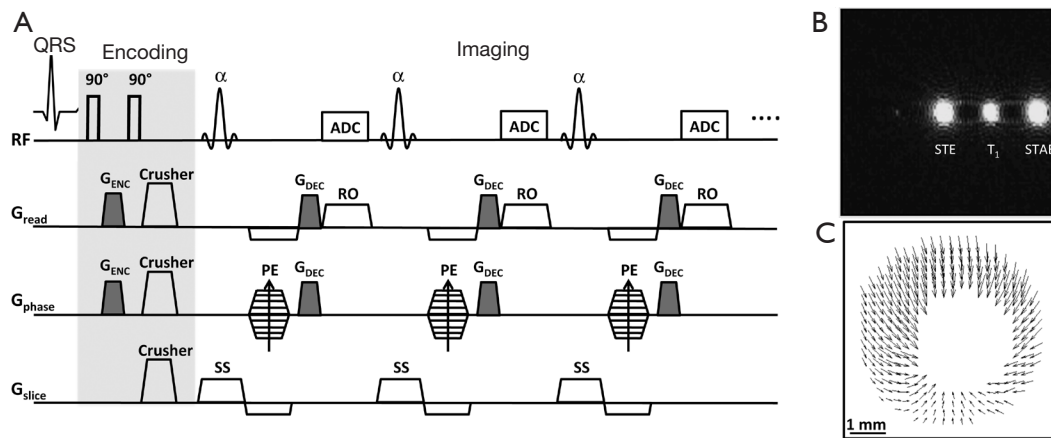


**Figure 4** DENSE CMR. (A) DENSE pulse sequence. A 1-1 SPAMM tagging module with encoding gradient  $G_{ENC}$  is used for displacement encoding. A stimulated echo (STE) is formed after the slice-selective RF pulse. A displacement decoding gradient  $G_{DEC}$  is applied to shift the stimulated echo to the center of k-space; (B) a representative DENSE image in k-space. Three echoes are formed: the STE, the  $T_1$  relaxation echo ( $T_1$ ), and the stimulated anti-echo (STAE); (C) a representative 2-D displacement map at peak systole by DENSE. [B is reproduced with permission from Epstein *et al.* (62)]. DENSE, displacement encoding with stimulated echoes; CMR, cardiovascular magnetic resonance; SPAMM, spatial modulation of magnetization; RF, radiofrequency.

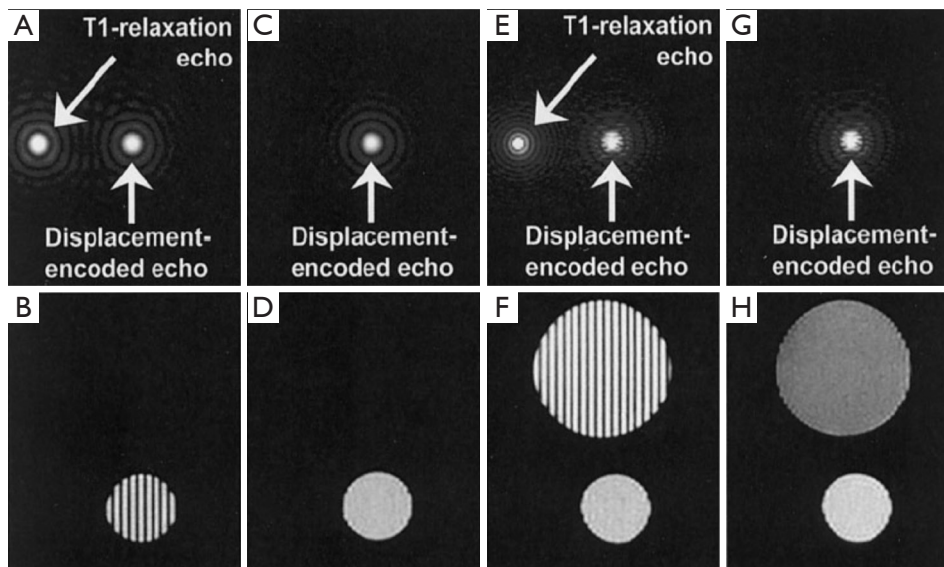


**Figure 5** Suppression of the  $T_1$  relaxation echo and stimulated anti-echo in DENSE. (A,B) A relatively large encoding gradient can eliminate the stimulated anti-echo but not the  $T_1$  relaxation echo (A). As a result, stripe artifacts occur in the magnitude-reconstructed image (B). (C,D) The inversion recovery (IR) method can effectively suppress the  $T_1$  relaxation echo if only a single  $T_1$  value is present (C) and the magnitude-reconstructed image is artifact-free (D). (E,F) The IR method fails to eliminate all  $T_1$  relaxation echoes when multiple  $T_1$  values are present (E) and thus stripe artifacts still occur in the reconstructed magnitude image (F). (G,H) The subtraction of complementary data sets can suppress the  $T_1$ -relaxation echo independently of  $T_1$  (G) and produce artifact-free images (H). [Reproduced with permission from Gilson *et al.* (63)]. DENSE, displacement encoding with stimulated echoes.

phase CSPAMM method (63). The subtraction of the two complementary displacement-encoded datasets produces artifact-free images (*Figure 5G,H*).

Another approach for echo suppression is the CANSSEL (Cosine ANd Sine acquisitions to ELIminate artifact generating echoes) acquisition scheme (62). In CANSSEL, four datasets are acquired by alternating the phase of both RF pulses in the SPAMM tagging module. The elimination of the stimulated anti-echo and the  $T_1$  relaxation echoes is realized by algebraic operation of these four datasets. Although the data acquisition time is prolonged, CANSSEL has the advantage of improved SNR and accuracy. Further, CANSSEL can be used in combination with the parallel imaging methods to shorten the scan time (65).

### Applications of MR tissue tagging and dense

MR tissue tagging and DENSE have been extensively used in both clinical and preclinical studies. They have been applied to measure regional wall motion mechanics in normal hearts and a spectrum of cardiac diseases such as coronary artery diseases, hypertrophic cardiomyopathy, and aortic stenosis, as well as diseases that may have an impact on cardiac function, such as Duchenne muscular dystrophies and diabetes.

#### Regional wall motion in normal hearts

A number of studies have reported transmural heterogeneity of strain patterns in humans. Specifically,  $E_{CC}$ ,  $E_{LL}$ , and  $E_{RR}$  have all been shown to increase from epicardium to endocardium (66–68). The same strain pattern was also observed in animal studies (69,70). In addition, maximum twist angle has also been shown to increase across the LV wall from epicardium towards the endocardium in both humans and animals. Although the similar trend of intramural heterogeneity in regional function exists in both human and animals, the study by Liu *et al.* demonstrated quantitative differences in regional ventricular wall motion in mice, rats, and humans (71). Their findings suggest that ventricular twist is conserved among the three species, leading to a significantly smaller torsion in humans as compared to mice and rats. In addition, both circumferential strain and normalized radial shortening were the largest in human subjects.

The effect of aging on normal myocardial function was also evaluated. Studies by Fonseca *et al.* (72) and Oxenham *et al.* (73) both reported a decrease in the peak rate of the

relaxation of circumferential and longitudinal strain and peak rate of torsion reversal in senescent hearts. In addition, Oxenham *et al.* also observed increased peak apical rotation and torsion during systole as well as significantly greater apical rotation, torsion, circumferential, and longitudinal strain persistence during myocardial relaxation and diastole in elderly subjects. Another study by Lumens *et al.* reported elevated systolic torsion to endocardial circumferential shortening ratio (torsion-to-shortening ratio; TSR) in elderly subjects, indicating that the transmural homogeneity of myofiber shortening is disrupted. In addition, they also observed mild concentric hypertrophy in the aged subjects, which may lead to subendocardial impairment. These findings suggest that aging may lead to more pronounced decrease of myofiber contraction in subendocardium than in subepicardium (74).

#### Coronary artery disease

Several studies have investigated the relationship between regional heart function and risk factors for atherosclerosis using CMR tagging. Edvardsen *et al.* have compared regional left ventricular systolic function to regional coronary calcium score measured by computed tomography (75). Their findings suggest that high local calcium score is associated with regional dysfunction in the corresponding coronary territory among individuals without a history of previous heart diseases, indicating a link between atherosclerosis and subclinical regional contractile dysfunction. Another study by Fernandes *et al.* reported that greater carotid intima-media thickness is associated with compromised systolic and diastolic function, suggesting a relationship between subclinical atherosclerosis and incipient myocardial dysfunction in a population free of clinical heart disease (76).

A number of studies have been conducted to investigate the relationship between myocardial ischemia and regional myocardial function. Studies by Kroeker *et al.* (77) and Garot *et al.* (78) found that myocardial ischemia can lead to a decrease in LV twist. Several studies demonstrated the importance of combining tagging with perfusion for evaluating ischemic heart disease (79–81). Sayad *et al.* reported that dobutamine CMR with myocardial tagging can quantitatively predict the recovery of regional function after revascularization (79). The study by Geskin *et al.* showed that the response of intramyocardial function to low-dose dobutamine after reperfusion can be quantified with MR tagging and that dysfunctional tissue after

myocardial infarction demonstrates a larger contractile response to dobutamine than normal myocardium (80). Kraitchman *et al.* also showed the importance of integrated CMR assessment of regional function and perfusion in a canine model of myocardial infarction (81).

Numerous studies have demonstrated the utility of MR tagging in the detection of myocardial infarction as well as in the evaluation of post-infarct ventricular remodeling. Götte *et al.* showed that strain analysis by tagging is more accurate than quantifying wall thickness in discriminating dysfunctional from functional myocardium (82). The study by Kramer *et al.* reported that LV dilatation and eccentric hypertrophy during remodeling are associated with persistent differences in segmental function between adjacent and remote non-infarcted regions in sheep hearts (83). Gerber *et al.* reported that in the early healing phase of acute myocardial infarction, the extent of microvascular obstruction in infarcted tissue was related to reduced local myocardial deformation and dysfunction of adjacent myocardium (84). Liu *et al.* also investigated the applicability and accuracy of HARP analysis for automatic strain quantification in rat hearts with myocardial infarction (54).

DENSE CMR has also been used to measure myocardial wall motion in post-infarct hearts. Aletras *et al.* used SENSE-accelerated DENSE CMR to detect abnormal myocardial deformation in patients with myocardial infarction (65). These investigators also performed a dog study to evaluate whether edema imaging can delineate the area at risk in reperfused hearts (85). DENSE has also been used to study the anatomical correlation between abnormal myocardial electromechanical events and infarct morphology in canine hearts (86). Further, Gilson *et al.* measured myocardial wall motion in mice before and after infarction using multi-slice DENSE (87). Later, they developed a modified DENSE sequence that can also detect contrast-enhanced infarcted myocardium from the magnitude images of the same DENSE dataset (64).

### ***Hypertrophic cardiomyopathy***

In hypertrophic cardiomyopathy, a portion of the LV wall is thickened and the blood pumping capacity of the ventricle is compromised. Hypertrophic cardiomyopathy is frequently asymptomatic until sudden cardiac death occurs (88). Therefore, diagnosis and intervention at early stage of the disease is of critical importance. MR tagging has been used to measure the LV regional functions in patients with hypertrophic cardiomyopathy. Maier *et al.* reported

a reduced radial displacement in the inferior septal region and a reduced cardiac rotation in the posterior region in patients with hypertrophic cardiomyopathy (89). Similarly changes were also observed and reported by Young *et al.* (90) and Dong *et al.* (91). In addition, Young *et al.* also observed increased ventricular torsion in patients with hypertrophic cardiomyopathy.

Hypertrophic cardiomyopathy can be caused by decreased expression of cardiac myosin binding protein C (cMyBPC) as a result of genetic mutations. A recent study by Desjardins *et al.* investigated the mechanisms that link cMyBPC expression and hypertrophic cardiomyopathy development in genetically manipulated mice using DENSE (92). They reported decreased LV torsion and circumferential strain, as well as circumferential strain rates in early systole and diastole in mice with both homogeneous and heterogeneous knockout of cMyBPC. Their results suggest that a modest decrease in cMyBPC expression in the mouse heart can lead to decreased contractile function that may contribute to the development of hypertrophic cardiomyopathy later in life.

### ***Aortic stenosis***

Aortic stenosis may lead to left ventricular hypertrophy and dysfunction. MR tagging has been used to investigate the impact of aortic stenosis on local myocardial motion. Stuber *et al.* observed increased apical twist and prolonged diastolic apical untwisting in patients with aortic stenosis, which may contribute to diastolic dysfunction (13). Sandstede *et al.* also performed a tagging study on patients with aortic stenosis to compare ventricular twist and contraction before and after valve replacement. They also observed similar increase in apical twist and ventricular torsion in patients before surgical valve replacement (93). However, ventricular torsion was normalized 1 year after the surgery. More recently, Mahmood *et al.* reported that cardiac steatosis was involved in the pathophysiology of aortic stenosis and can also be reversed by valve replacement (94). In another study, these investigators also reported the association of severe aortic stenosis and abnormal myocardial energetics caused by impaired perfusion reserve and myocardial oxygenation (95). However, these changes were reversible upon relief of pressure overload and hypertrophy regression.

### ***Muscular dystrophy***

Muscular dystrophy is an inherited disease characterized

by early onset of skeletal muscle degeneration and progressive weakness. However, early cardiac dysfunction is frequently undetected due to physical inactivity and generalized debilitation. Ashford *et al.* measured myocardial strain and torsion in pediatric subjects with Duchenne muscular dystrophy but without clinically apparent heart disease (96). They reported reduced mid-ventricular and basal circumferential strain in patients. Interestingly, Li *et al.* observed a biphasic change in myocardial wall strain and torsion in dystrophin-deficient mdx mice, a mouse model of Duchenne muscular dystrophy. Specifically, there was an initial increase in myocardial wall strain and torsion at young age, followed by progressive decrease at older ages (11). In both the human and the mouse studies, clinically used functional indexes of global ventricular function, such as ejection fraction, were normal. Hence, these two studies also demonstrated the sensitivity of CMR tagging to functional alterations over the global functional parameters.

## Conclusions

MR tagging and DENSE provide the opportunity for non-invasive and accurate measurement of regional myocardial wall motion. Although developed independently, MR tagging and DENSE share many similarities in pulse sequence and post-processing. The wide array of studies using MR tagging and DENSE in both clinical and preclinical investigation has demonstrated their capability in the delineation of normal myocardial wall motion patterns, the diagnosis of cardiac diseases, and the elucidation of the underlying mechanisms of disease development. In addition, with the advance in fast imaging technology and post-processing tools, the capabilities of these CMR techniques will be further improved and their application will also further enhance our understanding of the mechanical complexities underlying the function of the normal and diseased hearts.

*Disclosure:* The authors declare no conflict of interest.

## References

1. World Health Organization. Global Status Report on noncommunicable diseases 2010. Geneva: World Health Organization, 2010.
2. Ingels NB, Daughters GT, Stinson EB, Alderman EL. Evaluation of methods for quantitating left ventricular segmental wall motion in man using myocardial markers as a standard. *Circulation* 1980;61:966-72.
3. Abidov A, Germano G, Hachamovitch R, Berman DS. Gated SPECT in assessment of regional and global left ventricular function: major tool of modern nuclear imaging. *J Nucl Cardiol* 2006;13:261-79.
4. Abraham TP, Dimaano VL, Liang H-Y. Role of tissue Doppler and strain echocardiography in current clinical practice. *Circulation* 2007;116:2597-609.
5. Geyer H, Caracciolo G, Abe H, Wilansky S, Carerj S, Gentile F, Nesser HJ, Khandheria B, Narula J, Sengupta PP. Assessment of myocardial mechanics using speckle tracking echocardiography: fundamentals and clinical applications. *J Am Soc Echocardiogr* 2010;23:351-69.
6. Zerhouni EA, Parish DM, Rogers WJ, Yang A, Shapiro EP. Human heart: tagging with MR imaging--a method for noninvasive assessment of myocardial motion. *Radiology* 1988;169:59-63.
7. Sengupta PP, Korinek J, Belohlavek M, Narula J, Vannan MA, Jahangir A, Khandheria BK. Left ventricular structure and function: basic science for cardiac imaging. *J. Am. Coll. Cardiol* 2006;48:1988-2001.
8. Shehata ML, Cheng S, Osman NF, Bluemke DA, Lima JA. Myocardial tissue tagging with cardiovascular magnetic resonance. *J Cardiovasc Magn Reson* 2009;11:55.
9. Edvardsen T, Rosen BD, Pan L, Jerosch-Herold M, Lai S, Hundley WG, Sinha S, Kronmal RA, Bluemke DA, Lima JA. Regional diastolic dysfunction in individuals with left ventricular hypertrophy measured by tagged magnetic resonance imaging--the Multi-Ethnic Study of Atherosclerosis (MESA). *Am Heart J* 2006;151:109-14.
10. Burns AT, McDonald IG, Thomas JD, Macisaac A, Prior D. Doin' the twist: new tools for an old concept of myocardial function. *Heart* 2008;94:978-83.
11. Li W, Liu W, Zhong J, Yu X. Early manifestation of alteration in cardiac function in dystrophin deficient mdx mouse using 3D CMR tagging. *J Cardiovasc Magn Reson* 2009;11:40.
12. Dong SJ, Hees PS, Huang WM, Buffer SA, Weiss JL, Shapiro EP. Independent effects of preload, afterload, and contractility on left ventricular torsion. *Am J Physiol* 1999;277:H1053-60.
13. Stuber M, Scheidegger MB, Fischer SE, Nagel E, Steinemann F, Hess OM, Boesiger P. Alterations in the Local Myocardial Motion Pattern in Patients Suffering From Pressure Overload Due to Aortic Stenosis. *Circulation* 1999;100:361-8.
14. Yeon SB, Reichek N, Tallant BA, Lima JA, Calhoun LP,

- Clark NR, Hoffman EA, Ho KK, Axel L. Validation of in vivo myocardial strain measurement by magnetic resonance tagging with sonomicrometry. *J Am Coll Cardiol* 2001;38:555-61.
15. Axel L, Dougherty L. MR imaging of motion with spatial modulation of magnetization. *Radiology* 1989;171:841-5.
  16. Zhong J, Liu W, Yu X. Characterization of three-dimensional myocardial deformation in the mouse heart: an MR tagging study. *J Magn Reson Imaging* 2008;27:1263-70.
  17. Axel L, Dougherty L. Heart wall motion: improved method of spatial modulation of magnetization for MR imaging. *Radiology* 1989;172:349-50.
  18. Mosher TJ, Smith MB. A DANTE tagging sequence for the evaluation of translational sample motion. *Magn Reson Med* 1990;15:334-9.
  19. McVeigh ER, Bolster BD. Improved sampling of myocardial motion with variable separation tagging. *Magn Reson Med* 1998;39:657-61.
  20. Herzka DA, Guttman MA, McVeigh ER. Myocardial tagging with SSFP. *Magn Reson Med* 2003;49:329-40.
  21. Valeti VU, Chun W, Potter DD, Araoz PA, McGee KP, Glockner JF, Christian TF. Myocardial tagging and strain analysis at 3 Tesla: comparison with 1.5 Tesla imaging. *J Magn Reson Imaging* 2006;23:477-80.
  22. Pattynama PM, Doornbos J, Hermans J, van der Wall EE, de Roos A. Magnetic resonance evaluation of regional left ventricular function. Effect of through-plane motion. *Invest Radiol* 1992;27:681-5.
  23. Fischer SE, McKinnon GC, Maier SE, Boesiger P. Improved myocardial tagging contrast. *Magn Reson Med* 1993;30:191-200.
  24. Fischer SE, McKinnon GC, Scheidegger MB, Prins W, Meier D, Boesiger P. True myocardial motion tracking. *Magn Reson Med* 1994;31:401-13.
  25. Reeder SB, McVeigh ER. Tag contrast in breath-hold CINE cardiac MRI. *Magn Reson Med* 1994;31:521-5.
  26. Epstein FH, Wolff SD, Arai AE. Segmented k-space fast cardiac imaging using an echo-train readout. *Magn Reson Med* 1999;41:609-13.
  27. Tang C, McVeigh ER, Zerhouni EA. Multi-shot EPI for improvement of myocardial tag contrast: comparison with segmented SPGR. *Magn Reson Med* 1995;33:443-7.
  28. Stuber M, Spiegel MA, Fischer SE, Scheidegger MB, Danias PG, Pedersen EM, Boesiger P. Single breath-hold slice-following CSPAMM myocardial tagging. *MAGMA* 1999;9:85-91.
  29. Reeder SB, Atalar E, Faranesh AZ, McVeigh ER. Multi-echo segmented k-space imaging: an optimized hybrid sequence for ultrafast cardiac imaging. *Magn Reson Med* 1999;41:375-85.
  30. Zwanenburg JJ, Kuijjer JP, Marcus JT, Heethaar RM. Steady-state free precession with myocardial tagging: CSPAMM in a single breathhold. *Magn Reson Med* 2003;49:722-30.
  31. Ibrahim el-SH, Stuber M, Schär M, Osman NF. Improved myocardial tagging contrast in cine balanced SSFP images. *J Magn Reson Imaging* 2006;24:1159-67.
  32. Peters DC, Epstein FH, McVeigh ER. Myocardial wall tagging with undersampled projection reconstruction. *Magn Reson Med* 2001;45:562-7.
  33. Ryf S, Kissinger KV, Spiegel MA, Börnert P, Manning WJ, Boesiger P, Stuber M. Spiral MR myocardial tagging. *Magn Reson Med* 2004;51:237-42.
  34. Sodickson DK, Manning WJ. Simultaneous acquisition of spatial harmonics (SMASH): fast imaging with radiofrequency coil arrays. *Magn Reson Med* 1997;38:591-603.
  35. Pruessmann KP, Weiger M, Scheidegger MB, Boesiger P. SENSE: sensitivity encoding for fast MRI. *Magn Reson Med* 1999;42:952-62.
  36. Pai VM, Axel L. Advances in MRI tagging techniques for determining regional myocardial strain. *Curr Cardiol Rep* 2006;8:53-8.
  37. Guttman MA, Prince JL, McVeigh ER. Tag and contour detection in tagged MR images of the left ventricle. *IEEE Trans Med Imaging* 1994;13:74-88.
  38. Axel L, Gonçalves RC, Bloomgarden D. Regional heart wall motion: two-dimensional analysis and functional imaging with MR imaging. *Radiology* 1992;183:745-50.
  39. Young AA. Model tags: direct three-dimensional tracking of heart wall motion from tagged magnetic resonance images. *Med Image Anal* 1999;3:361-72.
  40. Hu Z, Metaxas D, Axel L. In vivo strain and stress estimation of the heart left and right ventricles from MRI images. *Med Image Anal* 2003;7:435-44.
  41. Pipe JG, Boes JL, Chenevert TL. Method for measuring three-dimensional motion with tagged MR imaging. *Radiology* 1991;181:591-5.
  42. Kuijjer JP, Marcus JT, Götte MJ, van Rossum AC, Heethaar RM. Three-dimensional myocardial strain analysis based on short- and long-axis magnetic resonance tagged images using a 1D displacement field. *Magn Reson Imaging* 2000;18:553-64.
  43. O'Dell WG, Moore CC, Hunter WC, Zerhouni EA, McVeigh ER. Three-dimensional myocardial

- deformations: calculation with displacement field fitting to tagged MR images. *Radiology* 1995;195:829-35.
44. Chen Y, Amini AA. A MAP framework for tag line detection in SPAMM data using Markov random fields on the B-spline solid. *IEEE Trans Med Imaging* 2002;21:1110-22.
  45. Huang J, Abendschein D, Dávila-Román VG, Amini AA. Spatio-temporal tracking of myocardial deformations with a 4-D B-spline model from tagged MRI. *IEEE Trans Med Imaging* 1999;18:957-72.
  46. Wang YP, Chen Y, Amini AA. Fast LV motion estimation using subspace approximation techniques. *IEEE Trans. Med. Imaging* 2001;20:499- 513.
  47. Amini AA, Chen Y, Elayyadi M, Radeva P. Tag surface reconstruction and tracking of myocardial beads from SPAMM-MRI with parametric B-spline surfaces. *IEEE Trans Med Imaging* 2001;20:94-103.
  48. Tustison NJ, Dávila-Román VG, Amini AA. Myocardial kinematics from tagged MRI based on a 4-D B-spline model. *IEEE Trans Biomed Eng* 2003;50:1038-40.
  49. Osman NF, Kerwin WS, McVeigh ER, Prince JL. Cardiac motion tracking using CINE harmonic phase (HARP) magnetic resonance imaging. *Magn Reson Med* 1999;42:1048-60.
  50. Zhong J, Liu W, Yu X. Transmural myocardial strain in mouse: quantification of high-resolution MR tagging using harmonic phase (HARP) analysis. *Magn Reson Med* 2009;61:1368-73.
  51. Osman NF, McVeigh ER, Prince JL. Imaging heart motion using harmonic phase MRI. *IEEE Trans Med Imaging* 2000;19:186-202.
  52. Garot J, Bluemke DA, Osman NF, Rochitte CE, McVeigh ER, Zerhouni EA, Prince JL, Lima JA. Fast determination of regional myocardial strain fields from tagged cardiac images using harmonic phase MRI. *Circulation* 2000;101:981-8.
  53. Garot J, Bluemke DA, Osman NF, Rochitte CE, Zerhouni EA, Prince JL, Lima JA. Transmural contractile reserve after reperfused myocardial infarction in dogs. *J Am Coll Cardiol* 2000;36:2339-46.
  54. Liu W, Chen J, Ji S, Allen JS, Bayly PV, Wickline SA, Yu X. Harmonic phase MR tagging for direct quantification of Lagrangian strain in rat hearts after myocardial infarction. *Magn Reson Med* 2004;52:1282-90.
  55. McVeigh ER, Zerhouni EA. Noninvasive measurement of transmural gradients in myocardial strain with MR imaging. *Radiology* 1991;180:677-83.
  56. Lima JA, Jeremy R, Guier W, Bouton S, Zerhouni EA, McVeigh E, Buchalter MB, Weisfeldt ML, Shapiro EP, Weiss JL. Accurate systolic wall thickening by nuclear magnetic resonance imaging with tissue tagging: correlation with sonomicrometers in normal and ischemic myocardium. *J Am Coll Cardiol* 1993;21:1741-51.
  57. Ryf S, Tsao J, Schwitter J, Stuessi A, Boesiger P. Peak-combination HARP: a method to correct for phase errors in HARP. *J Magn Reson Imaging* 2004;20:874-80.
  58. Kuijter JP, Jansen E, Marcus JT, van Rossum AC, Heethaar RM. Improved harmonic phase myocardial strain maps. *Magn Reson Med* 2001;46:993-9.
  59. Sampath S, Derbyshire JA, Atalar E, Osman NF, Prince JL. Real-time imaging of two-dimensional cardiac strain using a harmonic phase magnetic resonance imaging (HARP-MRI) pulse sequence. *Magn Reson Med* 2003;50:154-63.
  60. Abd-Elmoniem KZ, Sampath S, Osman NF, Prince JL. Real-time monitoring of cardiac regional function using fastHARP MRI and region-of-interest reconstruction. *IEEE Trans Biomed Eng* 2007;54:1650-6.
  61. Aletras AH, Ding S, Balaban RS, Wen H. DENSE: displacement encoding with stimulated echoes in cardiac functional MRI. *J Magn Reson* 1999;137:247-52.
  62. Epstein FH, Gilson WD. Displacement-encoded cardiac MRI using cosine and sine modulation to eliminate (CANSEL) artifact-generating echoes. *Magn Reson Med* 2004;52:774-81.
  63. Gilson WD, Yang Z, French BA, Epstein FH. Complementary displacement-encoded MRI for contrast-enhanced infarct detection and quantification of myocardial function in mice. *Magn Reson Med* 2004;51:744-52.
  64. Aletras AH, Wen H. Mixed echo train acquisition displacement encoding with stimulated echoes: an optimized DENSE method for in vivo functional imaging of the human heart. *Magn Reson Med* 2001;46:523-34.
  65. Aletras AH, Ingkanisorn WP, Mancini C, Arai AE. DENSE with SENSE. *J Magn Reson* 2005;176:99-106.
  66. Moore CC, Lugo-Olivieri CH, McVeigh ER, Zerhouni EA. Three-dimensional systolic strain patterns in the normal human left ventricle: characterization with tagged MR imaging. *Radiology* 2000;214:453-66.
  67. Kuijter JP, Marcus JT, Götte MJW, van Rossum AC, Heethaar RM. Three-dimensional myocardial strains at end-systole and during diastole in the left ventricle of normal humans. *J. Cardiovasc Magn Reson* 2002;4:341-51.
  68. Young AA, Kramer CM, Ferrari VA, Axel L, Reichek N. Three-dimensional left ventricular deformation in hypertrophic cardiomyopathy. *Circulation* 1994;90:854-67.

69. Aletras AH, Tilak GS, Natanzon A, Hsu LY, Gonzalez FM, Hoyt RF, Arai AE. Retrospective determination of the area at risk for reperfused acute myocardial infarction with T2-weighted cardiac magnetic resonance imaging: histopathological and displacement encoding with stimulated echoes (DENSE) functional validations. *Circulation* 2006;113:1865-70.
70. Zhong J, Yu X. Strain and torsion quantification in mouse hearts under dobutamine stimulation using 2D multiphase MR DENSE. *Magn Reson Med* 2010;64:1315-22.
71. Liu W, Ashford MW, Chen J, Watkins MP, Williams TA, Wickline SA, Yu X. MR tagging demonstrates quantitative differences in regional ventricular wall motion in mice, rats, and men. *Am J Physiol Heart Circ Physiol* 2006;291:H2515-21.
72. Fonseca CG, Oxenham HC, Cowan BR, Occleshaw CJ, Young AA. Aging alters patterns of regional nonuniformity in LV strain relaxation: a 3-D MR tissue tagging study. *Am J Physiol Heart Circ Physiol* 2003;285:H621-30.
73. Oxenham HC, Young AA, Cowan BR, Gentles TL, Occleshaw CJ, Fonseca CG, Doughty RN, Sharpe N. Age-Related Changes in Myocardial Relaxation Using Three-Dimensional Tagged Magnetic Resonance Imaging. *J Cardiovasc Magn Reson* 2003;5:421-30.
74. Lumens J, Delhaas T, Arts T, Cowan BR, Young AA. Impaired subendocardial contractile myofiber function in asymptomatic aged humans, as detected using MRI. *Am J Physiol Heart Circ Physiol* 2006;291:H1573-9.
75. Edvardsen T, Detrano R, Rosen BD, Carr JJ, Liu K, Lai S, Shea S, Pan L, Bluemke DA, Lima JA. Coronary artery atherosclerosis is related to reduced regional left ventricular function in individuals without history of clinical cardiovascular disease: the Multiethnic Study of Atherosclerosis. *Arterioscler Thromb Vasc Biol* 2006;26:206-11.
76. Fernandes VR, Polak JF, Edvardsen T, Carvalho B, Gomes A, Bluemke DA, Nasir K, O'Leary DH, Lima JA. Subclinical atherosclerosis and incipient regional myocardial dysfunction in asymptomatic individuals: the Multi-Ethnic Study of Atherosclerosis (MESA). *J Am Coll Cardiol* 2006;47:2420-8.
77. Kroeker CA, Tyberg JV, Beyar R. Effects of ischemia on left ventricular apex rotation. An experimental study in anesthetized dogs. *Circulation* 1995;92:3539-48.
78. Garot J, Pascal O, Diébold B, Derumeaux G, Gerber BL, Dubois-Randé JL, Lima JA, Guéret P. Alterations of systolic left ventricular twist after acute myocardial infarction. *Am J Physiol Heart Circ Physiol* 2002;282:H357-62.
79. Sayad DE, Willett DL, Hundley WG, Grayburn PA, Peshock RM. Dobutamine magnetic resonance imaging with myocardial tagging quantitatively predicts improvement in regional function after revascularization. *Am J Cardiol* 1998;82:1149-51, A10.
80. Geskin G, Kramer CM, Rogers WJ, Theobald TM, Pakstis D, Hu YL, Reichek N. Quantitative assessment of myocardial viability after infarction by dobutamine magnetic resonance tagging. *Circulation* 1998;98:217-23.
81. Kraitchman DL, Young AA, Bloomgarden DC, Fayad ZA, Dougherty L, Ferrari VA, Boston RC, Axel L. Integrated MRI assessment of regional function and perfusion in canine myocardial infarction. *Magn Reson Med* 1998;40:311-26.
82. Götte MJ, van Rossum AC, Twisk JW, Kuijper JP, Marcus JT, Visser CA. Quantification of regional contractile function after infarction: strain analysis superior to wall thickening analysis in discriminating infarct from remote myocardium. *J Am Coll Cardiol* 2001;37:808-17.
83. Kramer CM, Rogers WJ, Theobald TM, Power TP, Petruolo S, Reichek N. Remote noninfarcted region dysfunction soon after first anterior myocardial infarction. A magnetic resonance tagging study. *Circulation* 1996;94:660-6.
84. Gerber BL, Rochitte CE, Melin JA, McVeigh ER, Bluemke DA, Wu KC, Becker LC, Lima JA. Microvascular obstruction and left ventricular remodeling early after acute myocardial infarction. *Circulation* 2000;101:2734-41.
85. Aletras AH, Tilak GS, Natanzon A, Hsu LY, Gonzalez FM, Hoyt RF, Arai AE. Retrospective determination of the area at risk for reperfused acute myocardial infarction with T2-weighted cardiac magnetic resonance imaging: histopathological and displacement encoding with stimulated echoes (DENSE) functional validations. *Circulation* 2006;113:1865-70.
86. Ashikaga H, Mickelsen SR, Ennis DB, Rodriguez I, Kellman P, Wen H, McVeigh ER. Electromechanical analysis of infarct border zone in chronic myocardial infarction. *Am J Physiol Heart Circ Physiol* 2005;289:H1099-105.
87. Gilson WD, Yang Z, French BA, Epstein FH. Measurement of myocardial mechanics in mice before and after infarction using multislice displacement-encoded MRI with 3D motion encoding. *Am J Physiol Heart Circ Physiol* 2005;288:H1491-7.
88. Maron BJ, Thompson PD, Puffer JC, McGrew CA,

- Strong WB, Douglas PS, Clark LT, Mitten MJ, Crawford MH, Atkins DL, Driscoll DJ, Epstein AE. Cardiovascular preparticipation screening of competitive athletes. A statement for health professionals from the Sudden Death Committee (clinical cardiology) and Congenital Cardiac Defects Committee (cardiovascular disease in the young), American Heart As. *Circulation* 1996;94:850-6.
89. Maier SE, Fischer SE, McKinnon GC, Hess OM, Krayenbuehl HP, Boesiger P. Evaluation of left ventricular segmental wall motion in hypertrophic cardiomyopathy with myocardial tagging. *Circulation* 1992;86:1919-28.
90. Young AA, Kramer CM, Ferrari VA, Axel L, Reichek N. Three-dimensional left ventricular deformation in hypertrophic cardiomyopathy. *Circulation* 1994;90:854-67.
91. Dong SJ, MacGregor JH, Crawley AP, McVeigh E, Belenkie I, Smith ER, Tyberg JV, Beyar R. Left ventricular wall thickness and regional systolic function in patients with hypertrophic cardiomyopathy. A three-dimensional tagged magnetic resonance imaging study. *Circulation* 1994;90:1200-9.
92. Desjardins CL, Chen Y, Coulton AT, Hoit BD, Yu X, Stelzer JE. Cardiac myosin binding protein C insufficiency leads to early onset of mechanical dysfunction. *Circ Cardiovasc Imaging* 2012;5:127-36.
93. Sandstede JJ, Johnson T, Harre K, Beer M, Hofmann S, Pabst T, Kenn W, Voelker W, Neubauer S, Hahn D. Cardiac systolic rotation and contraction before and after valve replacement for aortic stenosis: a myocardial tagging study using MR imaging. *AJR Am J Roentgenol* 2002;178:953-8.
94. Mahmood M, Bull S, Suttie JJ, et al. Myocardial steatosis and left ventricular contractile dysfunction in patients with severe aortic stenosis. *Circ Cardiovasc Imaging* 2013;6:808-16.
95. Mahmood M, Francis JM, Pal N, et al. Myocardial perfusion and oxygenation are impaired during stress in severe aortic stenosis and correlate with impaired energetics and subclinical left ventricular dysfunction. *J Cardiovasc Magn Reson* 2014;16:29.
96. Ashford MW, Liu W, Lin SJ, Abraszewski P, Caruthers SD, Connolly AM, Yu X, Wickline SA. Occult cardiac contractile dysfunction in dystrophin-deficient children revealed by cardiac magnetic resonance strain imaging. *Circulation* 2005;112:2462-7.

**Cite this article as:** Jiang K, Yu X. Quantification of regional myocardial wall motion by cardiovascular magnetic resonance. *Quant Imaging Med Surg* 2014;4(5):345-357. doi: 10.3978/j.issn.2223-4292.2014.09.01